

Current-induced superconducting anisotropy of Sr_2RuO_4

R. Araki,^{1,*} T. Miyoshi,¹ H. Suwa,¹ E. I. Paredes Aulestia,² K. Y. Yip,²
Kwing To Lai,² S. K. Goh,² Y. Maeno,¹ and S. Yonezawa^{1,†}

¹*Department of Physics, Kyoto University, Kyoto 606-8502, Japan*

²*Department of Physics, The Chinese University of Hong Kong, Shatin N.T., Hong Kong*

(Dated: November 12, 2021)

In the unconventional superconductor Sr_2RuO_4 , unusual first-order superconducting transition has been observed in the low-temperature and high-field region, accompanied by a four-fold anisotropy of the in-plane upper critical magnetic field H_{c2} . The origin of such unusual H_{c2} behavior should be closely linked to the debated superconducting symmetry of this oxide. Here, toward clarification of the unusual H_{c2} behavior, we performed the resistivity measurements capable of switching in-plane current directions as well as precisely controlling the field directions. Our results reveal that resistive H_{c2} under the in-plane current exhibits an additional two-fold anisotropy. By systematically analyzing H_{c2} data taken under various current directions, we succeeded in separating the two-fold H_{c2} component into the one originating from applied current and the other originating from certain imperfection in the sample. The former component, attributable to vortex flow effect, is weakened at low temperatures where H_{c2} is substantially suppressed. The latter component is enhanced in the first order transition region, possibly reflecting a change in the nature of the superconducting state under high magnetic field.

INTRODUCTION

The layered perovskite superconductor Sr_2RuO_4 with the transition temperature T_c of 1.5 K [1] has been extensively studied due to its unconventional pairing state. Its Fermi surface has a relatively simple topology, consisting of three cylindrical sheets (α , β , and γ) [2, 3] with its well-characterized Fermi-liquid behavior. Recent nuclear magnetic resonance (NMR) experiments using low rf pulses revealed a technical problem in previous reports and clarified a reduction of the ^{17}O Knight shift in the superconducting states [4–6]. Recent polarized neutron scattering experiments performed under lower fields also revealed the reduction in the magnetic susceptibility in the Ru site [7]. These results cannot be explained in the framework of the traditional spin-triplet superconductivity scenario. Zero-field muon spin rotation (μSR) as well as magneto-optic Kerr effect experiments showed evidence for time-reversal-symmetry breaking (TRSB) [8, 9]. Recent μSR experiments under uniaxial stress reveal stress-induced splitting between the onset temperatures of superconductivity and TRSB [10] whereas such splitting does not occur as long as the tetragonal symmetry is preserved [11]. Furthermore, ultrasound measurements show that the superconducting order parameter of Sr_2RuO_4 consists of at least two components [10, 12, 13]. More recently, it is revealed that the NMR spectrum near the upper critical magnetic field H_{c2} exhibits characteristic “double-horn” structure, indicating the superconducting spin smecticity [14]. This result suggests that Sr_2RuO_4 is a strong candidate for the formation of the Fulde-Ferrell-Larkin-Ovchinnikov (FFLO) state [15, 16].

Toward clarification of the debated superconducting order parameter of Sr_2RuO_4 , properties near H_{c2} is of primary importance. Indeed, the superconducting transition becomes the first-order transition (FOT) under magnetic fields aligned accurately in the ab plane and below 0.8 K [17, 18]. Considering the recent revival of the NMR data, this first-order tran-

sition can be well interpreted as a consequence of the Pauli-paramagnetic pair-breaking effect, which is not allowed in the traditional chiral- p -wave spin-triplet scenario. More interestingly, in the same temperature region, $H_{c2//ab}$ exhibits a clear four-fold in-plane anisotropy [18–20]. Although this four-fold anisotropy preserves the tetragonal crystalline symmetry, its origin and relation to the first-order transition have not been clarified. The motivation of our study is to reveal the relationship between the $H_{c2//ab}$ anisotropy and FOT.

We focus on the anisotropy of H_{c2} in the ab plane under in-plane currents. First of all, H_{c2} under currents is expected to show the same four-fold symmetry as that under zero current [18–20]. Secondly, since type-II superconductors under currents and magnetic fields above the lower critical field H_{c1} exhibit vortex flow resistivity caused by the Lorentz force [21], H_{c2} in the ab plane of Sr_2RuO_4 is also expected to exhibit current-induced two-fold symmetry depending on the relative angle $\phi_H - \phi_I$ between the magnetic field H and current I . Here, ϕ_H and ϕ_I are the in-plane angles of the field and current with respect to the crystal axes, respectively. Thirdly, H_{c2} under currents may also depend on ϕ_I . Furthermore, these anisotropies of H_{c2} under currents are expected to show different behavior between the FOT and second-order transition (SOT) regions due to the difference in the dominant pair-breaking mechanisms. Thus, we consider the direction and strength of the current as new parameters of controlling H_{c2} , and extensively investigate the temperature dependence of the anisotropies of H_{c2} .

In order to clarify the electric current effect on the anisotropy of H_{c2} , it is crucial to identify and eliminate the effects of technical origins. First, because the value of $H_{c2//c}$ is about one twentieth less than that of $H_{c2//ab}$ [20], the presence of a small misalignment of in-plane magnetic field itself can lead to an apparent two-fold anisotropy of H_{c2} in the ab plane. Second, since the distribution of currents depends on the shape and distortion of the sample device, they can cause

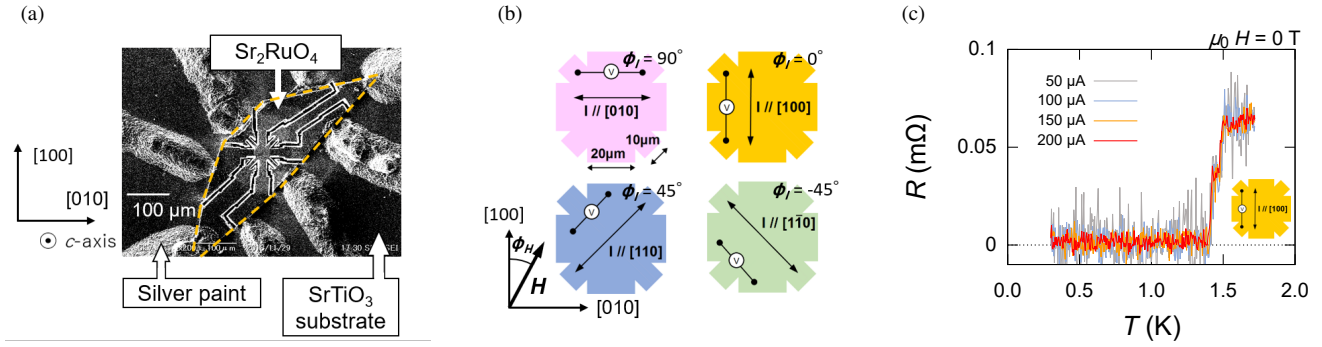


FIG. 1. Current-direction switchable device of single-crystalline Sr_2RuO_4 for H_{c2} -anisotropy measurements. (a) Scanning electron microscope (SEM) image of the device after the focused ion-beam (FIB) process. FIB-cut trenches are visible as black lines with white edges. The orange broken line indicates the original shape of the Sr_2RuO_4 crystal. To obtain low contact resistance, we used high-temperature-cure silver paint (Dupont, 6838). (b) Schematics of the four configurations of resistivity measurements with different current directions under magnetic fields. The $[100]$ direction is defined as $\phi = 0^\circ$ and the $[010]$ direction as $\phi = 90^\circ$ for both the field angle ϕ_H and current angle ϕ_I . (c) Resistive transition of the device measured on warming under zero field. The superconducting transition temperature T_c (1.45 K) remains close to the value for the cleanest samples (1.5 K) [22] even after the FIB process, and T_c does not depend on current below 200 μA .

apparent anisotropy dependent on the direction of the current ϕ_I . To avoid detecting these extrinsic anisotropies, we established a measurement procedure in which magnetic fields are applied in the ab plane accurately and precisely, and currents can be switched in various crystal orientations.

In this work, we measured resistivity of a micro-structured single-crystalline Sr_2RuO_4 sample under various in-plane field and current directions. The sample was processed by focused ion-beam (FIB) as shown in Fig. 1(a); this structured sample allows us to switch the current in the $[100]$, $[010]$, $[110]$ and $[1\bar{1}0]$ directions. We find that, with a given current direction, H_{c2} exhibits two-fold anisotropy as a function of the in-plane field angle, in addition to the ordinary four-fold anisotropy. Careful analysis reveals that the two-fold component consists of two contributions: the one caused by external current likely due to vortex-flow effect, and the other originating from sample inhomogeneity probably introduced by the FIB process. We revealed that the latter is enhanced below 0.8 K, namely in the FOT regime, attributable to a change in the superconducting order parameter.

EXPERIMENTAL

In this study, we used Sr_2RuO_4 single crystals grown with the floating-zone method [23]. Before the micro-fabrication of the resistivity device, T_c of a thin crystal (batch: C432; $500 \mu\text{m} \times 100 \mu\text{m} \times 10 \mu\text{m}$) was measured to be 1.43 K (see Supplemental Material (SM) [24]), defined as the peak of the imaginary part of the AC susceptibility measured using a compact susceptometer [25] that fits inside a commercial refrigerator (Quantum Design; PPMS adiabatic demagnetization refrigerator option). The crystalline orientation of the sample was determined by x-ray Laue pictures.

The crystal was placed on a single-crystalline SrTiO_3 substrate (Shinkosha), which has a thermal contraction matching with that of Sr_2RuO_4 [26, 27]. After the electrical contact between the Sr_2RuO_4 crystal and eight electrodes, made of high-temperature-cure silver paint (Dupont, 6838), were established similarly to previous studies [28], the surface of the crystal was protected by evaporating a $0.5\text{-}\mu\text{m}$ layer of SiO_x . We then used a focused ion beam (FIB) instrument (JEOL, JIM-4501) with a Ga ion beam to fabricate the current-direction switchable resistivity device. Figure 1(a) shows a scanning electron microscope (SEM) image of the device taken from the c -axis direction. As shown in the figure, the widths of the arms along the $[100]$ and $[010]$ directions are both $20 \mu\text{m}$, and those along the $[110]$ and $[1\bar{1}0]$ directions are $10 \mu\text{m}$. The device thickness is $10 \mu\text{m}$.

The Sr_2RuO_4 device was cooled down to 0.12 K with a ^3He - ^4He dilution refrigerator (Oxford Instruments, Kelvinox 25). For controlling the field orientation at low temperatures, we used a vector magnet system (Cryomagnetics, VSC-3050) with orthogonally arranged SC magnets that generate a horizontal field H_r of up to 5 T and a vertical field H_z of up to 3 T to control the polar field angle $\theta_{\text{lab}} = \arctan(H_z/H_r)$ [29]. This vector magnet allows control of θ_{lab} with a typical precision of $\Delta\theta_{\text{lab}} = 0.005^\circ$ at $\mu_0 H = 1$ T. Moreover, the magnet set is placed on a horizontal rotation stage, which can control the azimuthal field angle ϕ_{lab} with a precision of $\Delta\phi_{\text{lab}} = 0.001^\circ$. The quasi-two-dimensional (2D) anisotropy of H_{c2} of Sr_2RuO_4 ($H_{c2//ab}/H_{c2//c} \sim 20$ [20]) allows us to align the field to the ab plane accurately and precisely: by rotating magnetic field close to $H_{c2//ab}$, we can find a sharp drop of resistivity when the field is exactly parallel to the ab plane (see SM [24]). The in-plane alignment was done based on the known four-fold anisotropy of the in-plane H_{c2} (i.e. $H_{c2//[110]} > H_{c2//[100]}$ below 0.8 K) [19, 20]. All the data shown in this paper are

plotted using the field angles ϕ_H and θ_H defined in the sample coordinate.

To measure the sample resistance R , we employed a DC method with current sign reversal to avoid influence of voltage offsets such as thermoelectric voltages. We used a combination of a current source (Keithley, 6221) and a nanovoltmeter (Keithley, 2182A). We measured R against various parameters: temperature T , magnitude and azimuthal angle of magnetic field H and ϕ_H , current amplitude and direction I and ϕ_I . Both ϕ_H and ϕ_I are defined with respect to the [100] direction as shown in Fig. 1(b). We note that for a given current value, the current density for an orthogonal measurement ($I/[100]$ or $[010]$) is half of that for a diagonal measurement ($I/[110]$ or $[1\bar{1}0]$) due to the larger width of the arm along the [100] or [010] directions.

Figure 1(c) shows the temperature dependence of R under zero field. The resistivity reaches zero at $T_c = 1.45$ K. The consistent T_c values before and after FIB assure that a possible damage or strain due to FIB is minimal. In this study we used the current values below 200 μ A for which T_c does not change under zero field.

RESULTS AND ANALYSIS

To investigate the anisotropy of the resistive H_{c2} in the ab plane under in-plane currents, we measured $R(H)$ under various field and current conditions. We show in Fig. 2 representative field dependence of the resistance for $I/[100]$. Additional raw data are shown in SM [24]. The in-plane H_{c2} , defined with the deviation from $R = 0$ as indicated by the arrows, clearly depends on the in-plane field direction and on the current strength.

Figures 3(a) and 3(c) compare the ϕ_H dependence of the in-plane H_{c2} for $I/[010]$ and $I/[100]$ measured at 200 μ A and 0.40 K. Under in-plane currents, $H_{c2}(\phi_H)$ clearly shows not only the known four-fold anisotropy but also an additional two-fold anisotropy. This is also evident in the raw data in Fig. 2: For example, H_{c2} for $\phi_H = 45^\circ$ is noticeably larger than that for $\phi_H = 135^\circ$, although these two conditions should be equivalent considering the tetragonal crystalline symmetry if the current were absent. We have confirmed that this two-fold behavior is not caused by the misalignment of fields with respect to the ab plane (Fig. S2 in SM [24]). Moreover, comparing Figs. 3(a) and (c), we notice that this two-fold components of H_{c2} are altered by changing the current direction ϕ_I . For example, the H_{c2} value at $\phi_H = 0^\circ$ is smaller than that at 90° for $I/[010]$ (Fig. 3(a)), whereas they are opposite for $I/[100]$ (Fig. 3(c)). This fact also evidences that the external current plays an important role in the observed two-fold behavior.

To analyze the two-fold behavior quantitatively, we fit the $H_{c2}(\phi_H)$ data with a combination of two and four-fold sinusoidal functions with a constant offset:

$$\mu_0 h_{c2}(\phi_H) = a_0 + a_2 \cos 2\phi_H + b_2 \sin 2\phi_H + a_4 \cos 4\phi_H. \quad (1)$$

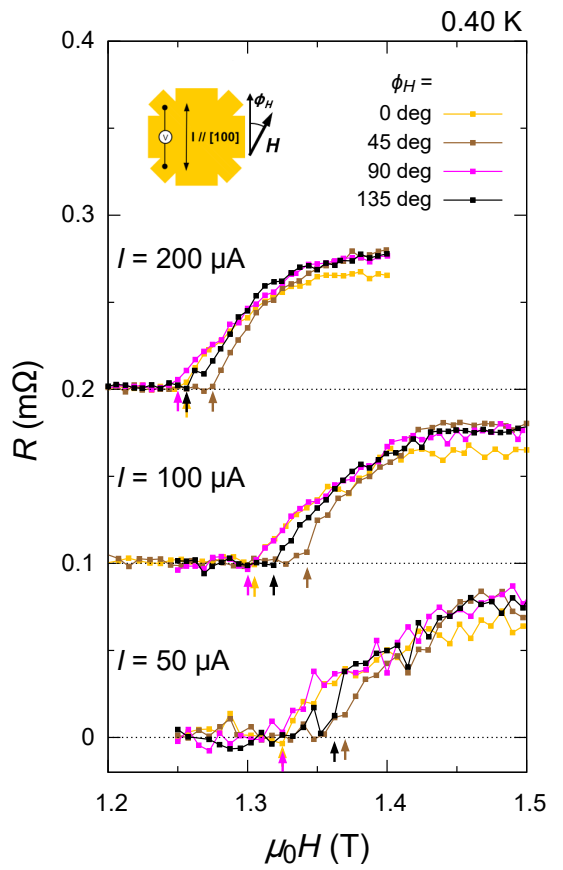


FIG. 2. Representative resistive transition of our Sr_2RuO_4 device under various values of in-plane currents I . These data were taken at 0.40 K with current along the [100] direction. The curves with $I \geq 100 \mu\text{A}$ have vertical offsets. The yellow, brown, pink and black data points are obtained under $\phi_H = 0^\circ, 45^\circ, 90^\circ$ and 135° , respectively. In addition to the known four-fold anisotropy, H_{c2} , indicated by the vertical arrows, exhibits two-fold anisotropy as evidenced by the differences in the curves between $\phi_H = 0^\circ$ and 90° , or between $\phi_H = 45^\circ$ and 135° .

We comment that the four-fold cosine term represents the known H_{c2} anisotropy under zero current ($H_{c2/[110]} > H_{c2/[100]}$) [19, 20] and we have checked that the four-fold sine term is negligible even under currents. As exemplified by the solid curves in Figs. 3(a) and (c), the fitting was successful for the $H_{c2}(\phi_H)$ data sets. The obtained value of a_4 is $\sim -0.011 \text{ T}$ and $\sim -0.010 \text{ T}$ for the data in Fig. 3(a) and (c). These values are consistent with the previous studies [19, 20]. Notice that the quantity $\Delta(\mu_0 H_{c2}) = \mu_0 H_{c2}[110] - \mu_0 H_{c2}[100]$ in the literature corresponds to the quantity $-2a_4$ of our study. Then, to extract the two-fold component $H_{c2}^{(2)}$, we subtracted the fitted four-fold component $a_4 \cos 4\phi_H$ and the offset a_0 from the data. The results are shown in Figs. 3(b) and (d). Here, the colored curves represent the two-fold terms obtained by the fitting, whereas the black solid and broken curves are decomposed $\cos 2\phi_H$ and $\sin 2\phi_H$ components, respectively. Between $I/[100]$ and $[010]$, $H_{c2}^{(2)}$ is clearly different with the

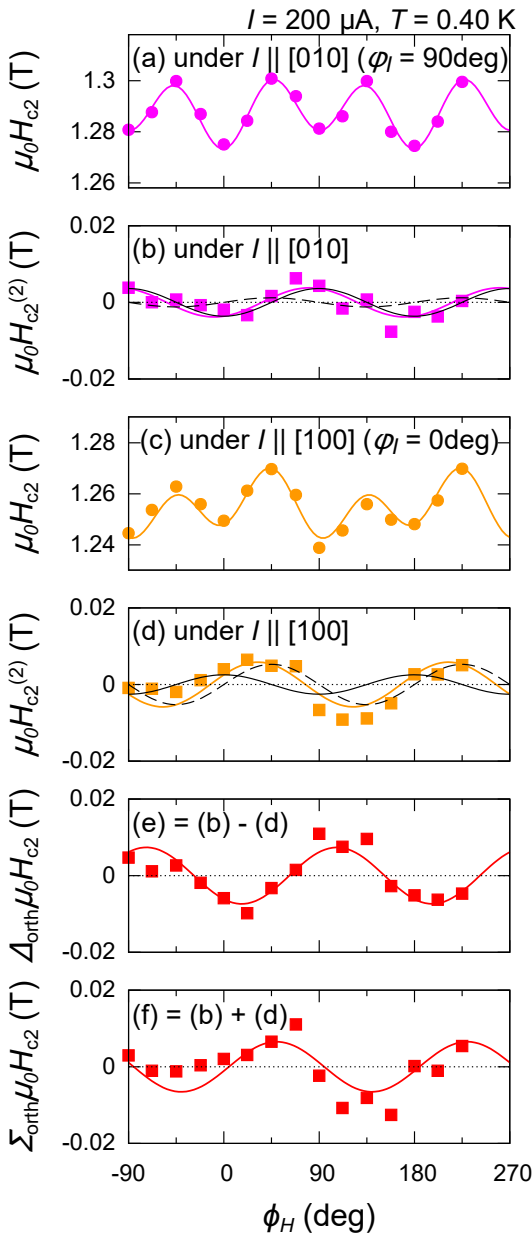


FIG. 3. H_{c2} anisotropy of Sr_2RuO_4 under in-plane current. Additional data are shown in SM [24]. (a) Raw H_{c2} data as a function of ϕ_H under current along the [010] direction. The data are well fitted with a combination of four-fold and two-fold sinusoidal function (Eq. (1)) as shown with the pink solid curve. (b) two-fold component of H_{c2} under $I/[010]$ (pink squares), extracted from the raw H_{c2} data by subtracting the fitted four-fold component and the constant offset. The pink curve present the two-fold sinusoidal fitting, whereas the solid and broken black curves show the decomposed cosine and sine terms of the pink curve, respectively. (c) Raw H_{c2} data (circles) and fitting result (solid curve) under current along the [100] direction. Compared to (a), the data suggest that current direction ϕ_I switches the sign of the difference between H_{c2} at $\phi_H = 0^\circ$ and that at $\phi_H = 90^\circ$. (d) two-fold component of H_{c2} under $I/[100]$ together with the two-fold fitting (orange curve) and the decomposed cosine (black solid curve) and sine (black broken curve) components. (e) I -induced two-fold component of H_{c2} obtained by taking the difference between the data in (b) and (d). This only contains the two-fold component that is switched by the change of the current direction. (f) I -independent two-fold component of H_{c2} obtained by taking the summation of the data in (b) and (d). This only contains the two-fold component that is not switched by the change of the current direction.

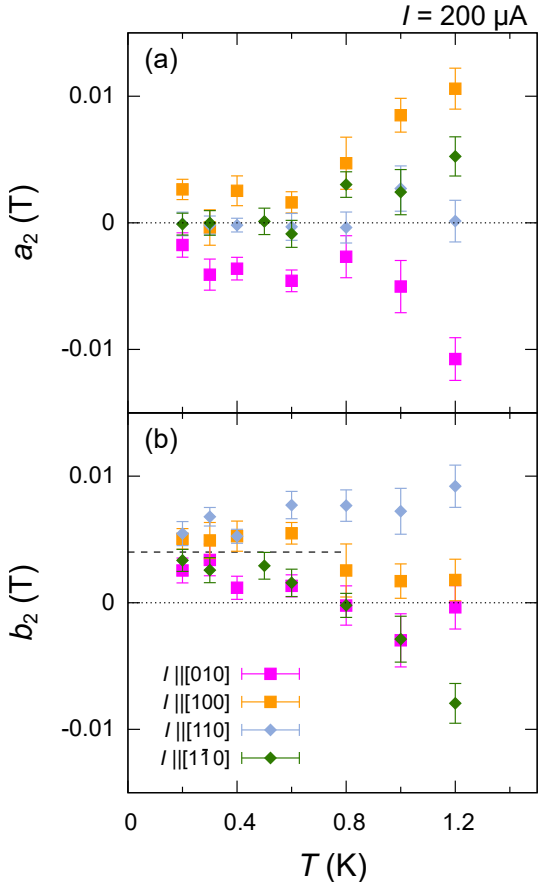


FIG. 4. Temperature dependence of $H_{c2}^{(2)}$ measured under current along the four directions. The pink, yellow, blue and green points correspond to [010], [100], [110] and [110] current directions. (a) Coefficient of the two-fold cosine component a_2 . a_2 under $I/[100]$ and [010] increases on warming and their signs are switched by current-directions. In contrast, a_2 under $I/[110]$ and [110] stays nearly zero. These results suggest that $H_{c2}^{(2)}$ is mostly induced by current and thus behaves as $\cos 2(\phi_H - \phi_I)$. (b) Coefficient of the two-fold sine component b_2 . Similar to a_2 , the current-direction dependence of b_2 at high temperature is consistent with the expectation $H_{c2}^{(2)} \propto \cos 2(\phi_H - \phi_I)$. However, unlike a_2 , b_2 under all current-directions have an additional term reaching nearly 0.005 T on cooling to 0 K.

opposite sign of the cosine component.

We present the T -dependence of the obtained fitting parameters a_2 and b_2 in eq. 1 for various current directions in Fig. 4. (Behavior of a_0 and a_4 will be discussed later.) For the coefficient of the $\cos 2\phi_H$ component a_2 , its magnitude under the orthogonal current directions, namely $I/[100]$ and $I/[010]$, increases on warming while its sign is switched by current-direction change. This is indeed expected for a current-induced effect, where by symmetry $H_{c2}^{(2)}$ should behave as $\propto \cos 2(\phi_H - \phi_I) = \cos 2\phi_H$ for $\phi_I = 0^\circ$ ($I/[100]$) and $-\cos 2\phi_H$ for $\phi_I = 90^\circ$ ($I/[010]$). In contrast, a_2 under the diagonal current directions, namely $I/[110]$ and $I/[1\bar{1}0]$, are nearly independent of temperature and stays close to zero.

This is again consistent with the $\cos 2(\phi_H - \phi_I)$ behavior for the current-induced $H_{c2}^{(2)}$, since $\cos 2(\phi_H - \phi_I) = \pm \sin 2\phi_H$ for $\phi_I = \pm 45^\circ$ and thus the cosine component should be zero. Figure 4(b) shows the temperature dependence of the coefficients b_2 . At high temperatures, the behavior of b_2 is similar to that of a_2 except for an exchange of the roles between the orthogonal and diagonal current directions: b_2 is finite and its sign depends on the current direction $I/[110]$ or $[1\bar{1}0]$, but is nearly zero for $I/[100]$ and $[010]$. Thus this high-temperature behavior in b_2 again indicate $H_{c2}^{(2)} \propto \cos 2(\phi_H - \phi_I)$ behavior. However, at lower temperatures, b_2 tends to converge to a finite value $b_2(T \rightarrow 0) \sim 0.005$ T irrespective of the current directions. Such convergence reveals an additional two-fold component that is not caused by external current.

From these analyses, we revealed that the $H_{c2}^{(2)}$ data have current-independent and current-dependent contributions, which we hereafter express as $H_{c2}^{(2\text{ind})}$ and $H_{c2}^{(2\text{dep})}$. The former corresponds to the low-temperature current-direction independent behavior in b_2 (Fig. 4(b)) and the latter corresponds to the $\cos 2(\phi_H - \phi_I)$ term as seen in the behavior common to a_2 and b_2 discussed in the previous paragraph. Further analyses and interpretations of these contributions will be provided in the next section.

Before closing this section, we comment on possible heating effects due to current. We estimate the upper limit of the actual sample temperature from the current dependence of the coefficient a_0 by assuming that its variation with current is solely due to Joule heating (see SM [24]). This estimation indicates that the temperature increase is at most 0.2 K in the lowest temperature region and less than 0.1 K above 0.4 K.

DISCUSSION

As explained in the previous section, we extracted two-fold anisotropy of H_{c2} of Sr_2RuO_4 under current. We reveal systematically how this additional anisotropy depends on current-strength, current-directions, and temperature. As a well-known effect, external current induces vortex flows in the mixed state by the Lorentz force, leading to the apparent reduction in H_{c2} . Thus, such an effect is maximized under field perpendicular to current and would not occur under field parallel to current; As a result, this effect is expressed as a two-fold cosine-like component $\propto \cos 2(\phi_H - \phi_I)$, whose sign is negative under field perpendicular to current (i.e. $\phi_H - \phi_I = \pm 90^\circ$) and positive under field parallel to current (i.e. $\phi_H = \phi_I$).

For ordinary type-II superconductors (both 2D and 3D) in which the main pair-breaking effect is the ordinary orbital effect, the vortex-flow effect is expected to be observed. However, in Sr_2RuO_4 , the FOT occurs below 0.8 K, indicating that the dominated pair-breaking effect is not the orbital effect. Thus, the two-fold cosine-like component can behave differently between the FOT and the SOT regions.

In order to extract the current-dependent term including the vortex-flow effect from the $H_{c2}^{(2)}$ data, we take the difference

between the $H_{c2}^{(2)}(\phi_H, \phi_I = 90^\circ)$ data and $H_{c2}^{(2)}(\phi_H, \phi_I = 0^\circ)$ data. This process is motivated by the following expectation. We expect that the two-fold component $H_{c2}^{(2)}(\phi_H, \phi_I)$ contain current-independent term $H_{c2}^{(2\text{ind})}(\phi_H)$ and current-dependent term $H_{c2}^{(2\text{dep})}(\phi_H - \phi_I)$, *i.e.*

$$H_{c2}^{(2)}(\phi_H, \phi_I) = H_{c2}^{(2\text{ind})}(\phi_H) + H_{c2}^{(2\text{dep})}(\phi_H - \phi_I). \quad (2)$$

Then, due to the two-fold nature, $H_{c2}^{(2\text{dep})}$ should change sign upon a current-direction switching of 90° , as

$$H_{c2}^{(2\text{dep})}(\phi_H - (\phi_I + 90^\circ)) = -H_{c2}^{(2\text{dep})}(\phi_H - \phi_I). \quad (3)$$

In contrast, $H_{c2}^{(2\text{ind})}$ is, by definition, independent of the 90° current direction switching. Thus, by calculating

$$\Delta_{\text{orth}} H_{c2}^{(2)} \equiv H_{c2}^{(2)}(\phi_I = 90^\circ) - H_{c2}^{(2)}(\phi_I = 0^\circ), \quad (4)$$

$H_{c2}^{(2\text{ind})}$ is eliminated and we can expect that $\Delta_{\text{orth}} H_{c2}^{(2)} \simeq 2H_{c2}^{(2\text{dep})}(\phi_I = 90^\circ)$. A representative $\Delta_{\text{orth}} H_{c2}^{(2)}$ is shown in Fig. 3(e). Similarly,

$$\Delta_{\text{diag}} H_{c2}^{(2)} \equiv H_{c2}^{(2)}(\phi_I = 45^\circ) - H_{c2}^{(2)}(\phi_I = -45^\circ) \quad (5)$$

should satisfy $\Delta_{\text{diag}} H_{c2}^{(2)} \simeq 2H_{c2}^{(2\text{dep})}$ (Fig. S4), providing an independent evaluation of $H_{c2}^{(2\text{dep})}(\phi_I = 45^\circ)$. On the other hand, we can extract the current-independent term $H_{c2}^{(2\text{ind})}(\phi_H)$ by evaluating sums of the datasets with 90° current switching:

$$\Sigma_{\text{orth}} H_{c2}^{(2)} \equiv H_{c2}^{(2)}(\phi_I = 90^\circ) + H_{c2}^{(2)}(\phi_I = 0^\circ) \quad (6)$$

and

$$\Sigma_{\text{diag}} H_{c2}^{(2)} \equiv H_{c2}^{(2)}(\phi_I = 45^\circ) + H_{c2}^{(2)}(\phi_I = -45^\circ). \quad (7)$$

In these sums, current-dependent terms are eliminated and we expect $\Sigma_{\text{orth}} H_{c2}^{(2)} \simeq \Sigma_{\text{diag}} H_{c2}^{(2)} \simeq 2H_{c2}^{(2\text{ind})}$. A representative $\Sigma_{\text{orth}} H_{c2}^{(2)}$ is shown in Fig. 3(f) and $\Sigma_{\text{diag}} H_{c2}^{(2)}$ in Fig. S4.

In Figs. 3(e), 3(f), S4, one can clearly see that $\Delta_{\text{orth}} H_{c2}^{(2)}$ and $\Delta_{\text{diag}} H_{c2}^{(2)}$ are dominated by $\cos 2(\phi_H - \phi_I)|_{\phi_I=90^\circ, 45^\circ}$ and $\Sigma_{\text{orth}} H_{c2}^{(2)}$ and $\Sigma_{\text{diag}} H_{c2}^{(2)}$ are by $\sin 2\phi_H$. To perform quantitative analysis, we fitted $(1/2)\Sigma H_{c2}^{(2)}$ by $A_2 \cos 2\phi_H + B_2 \sin 2\phi_H$ and $(1/2)\Delta H_{c2}^{(2)}$ by $C_2 \cos 2(\phi_H - \phi_I)|_{\phi_I=90^\circ, 45^\circ} + D_2 \sin 2(\phi_H - \phi_I)|_{\phi_I=90^\circ, 45^\circ}$. The resultant parameters are plotted in Figs. 5(c), (d), S6(a) and S6(b). We confirmed that the coefficients evaluated from the orthogonal and diagonal combinations agree with each other, manifesting the validity of the analyses. We then indeed find A_2 and D_2 are small and do not exhibit temperature dependence. In contrast, B_2 and C_2 plotted in Figs. 5(c) and (d) are much larger than A_2 or D_2 and exhibits characteristic temperature dependence as will be discussed later.

In Figs. 5(a) and (b) the angle-independent component a_0 (see Eq. (1)) and four-fold component $-2a_4$ are compared with the coefficients B_2 and C_2 . Notice that the coefficient a_0 in Eq. (1) can be considered as the in-plane average H_{c2}

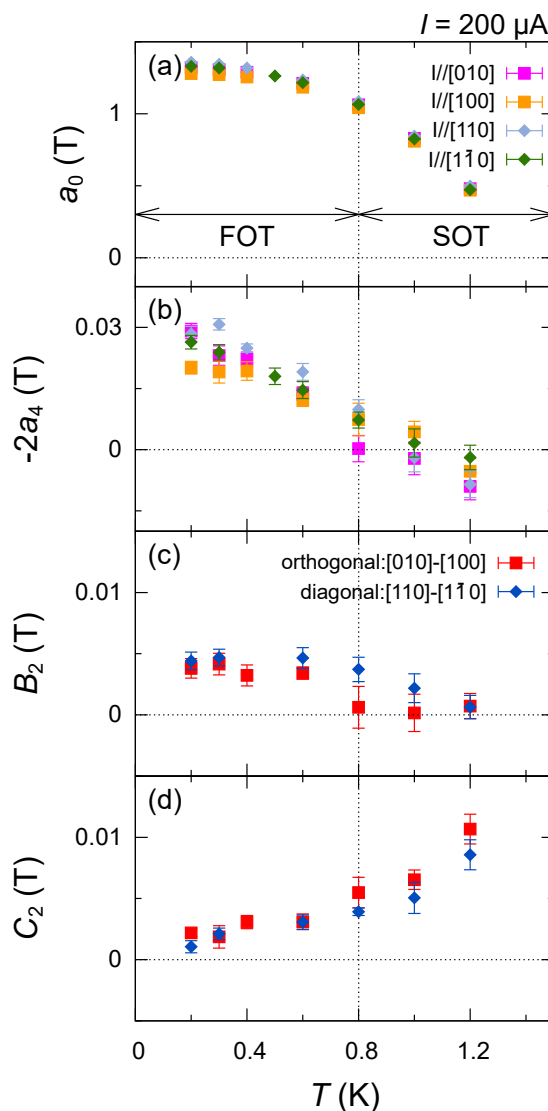


FIG. 5. Relation among the first-order transition (FOT) region and H_{c2} anisotropies under current. (a) T -dependence of a_0 . Since a_0 corresponds to the in-plane average value of H_{c2} , this curve provide the H_{c2} - T phase diagram of this sample. (b) T -dependence of the four-fold component $-2a_4$. The behavior of $-2a_4$ is consistent with the previous studies [19, 20]. In (a) and (b), the pink, orange, sky-blue and green points are for the data obtained with $I/[010]$, $[100]$, $[110]$ and $[1\bar{1}0]$, respectively. (c) and (d); T -dependence of two-fold I -independent component and I -dependent component of $H_{c2}^{(2)}$. Red squares and blue diamonds are the data obtained for orthogonal and diagonal current-directions, respectively. The two-fold I -independent sine component B_2 reaches about 0.005 T in the FOT region ($T \leq 0.8$ K) and nearly zero in the second-order transition region ($T \geq 0.8$ K). This result indicates that the sample in a high-field state becomes more sensitive to inhomogeneity effect, producing two-fold anisotropy. The $\cos 2(\phi_H - \phi_I)$ component C_2 in (d) increase on warming. This observation is consistent with vortex flow effect.

and thus provide the H_{c2} - T phase diagram of Sr_2RuO_4 . Indeed, Fig. 5(a) agrees well with the phase diagram reported in literature [18, 20]. The value $-2a_4$ should be equal to $\mu_0 H_{c2/[110]} - \mu_0 H_{c2/[100]}$ in the absence of current, characterizing the known four-fold H_{c2} anisotropy. This quantity is nearly zero above 0.8 K but increase on cooling in the FOT region and reaches 0.03 T at the lowest temperature. Such behavior is consistent with the previous studies.

As shown in Fig. 5(d), the coefficient C_2 exhibits a finite value and decreases on cooling. The coefficient D_2 exhibits a smaller value than C_2 and show only a weak temperature dependence (see SM [24]). These results indicate that the current-dependent components are cosine-like and increase on warming. It is consistent with the scenario where vortex flow gives current-dependent two-fold anisotropy of H_{c2} .

The coefficient B_2 shown in Fig. 5(c), characterizing current-independent two-fold behavior, is finite only below 0.8 K in the FOT region, for the orthogonal current. A similar tendency is clear for the diagonal current. Since other bulk measurements have not revealed such a current-independent two-fold component of H_{c2} , the behavior of B_2 is probably related to minute surface damage caused by the FIB processing. However, it is not sufficient to explain the T -dependence of B_2 because it does not change smoothly but appear only in the FOT region. This behavior can be explained if the resistivity suddenly becomes more sensitive to the inhomogeneity in the FOT region. One possible candidate for such sudden change in the resistivity property is the formation of the FFLO state, which is accompanied by a real-space modulation of the superconducting order parameter and is recently revealed by an NMR experiment [30]. If there is a surface damage, for example, the FFLO order-parameter modulation can be pinned to the surface damage and such pinning can induce additional two-fold behavior in $H_{c2}(\phi_H)$.

SUMMARY AND CONCLUSION

Here we summarize the main results of our study.

(1) The angle-independent component a_0 in Eq. (1) can be considered as the in-plane average H_{c2} .

(2) The quantity $-2a_4$ characterizes the known four-fold H_{c2} anisotropy. It corresponds to $\Delta(\mu_0 H_{c2})$ in the previous studies [19, 20] and exhibits about 80% of the value of $\Delta(\mu_0 H_{c2})$ in the first-order transition region. In the second-order transition region, $-2a_4$ shows close to zero in the same way as $\Delta(\mu_0 H_{c2})$. Thus, the four-fold anisotropy in H_{c2} under in-plane current shows the same T -dependence as that of the four-fold anisotropy in H_{c2} under zero current.

(3) The coefficient C_2 shows the $\cos 2(\phi_H - \phi_I)$ component of $H_{c2}^{(2\text{dep})}$. Since it takes positively finite values and increases with temperature, the current-induced two-fold anisotropy in $H_{c2}^{(2)}$ is probably due to the vortex-flow effect.

(4) The coefficient B_2 shows the two-fold I -independent sine component of $H_{c2}^{(2)}$. Such a two-fold component has not been observed in previous experiments [18–20]. This quan-

ity revealed in our study becomes finite only in the first-order transition region. This is probably related to minute the crystal distortion and surface damage caused by FIB processing. However, it is not enough to explain why B_2 becomes finite only in the first-order transition region. As a possible scenario, we propose that the increased sensitivity to inhomogeneity is due to the realization of FFLO state in the first-order transition region.

In conclusion, we have established a clear approach to probe the electrical resistivity of two-dimensional superconductors, such as Sr_2RuO_4 , with a varying current and magnetic field directions. The combination of the vector magnet and our FIB structured sample enables us to control the azimuthal field angle ϕ_H , and switch in-plane current-direction ϕ_I along four crystal orientations. We have demonstrated that H_{c2} in the ab plane of Sr_2RuO_4 exhibits not only an ordinary four-fold anisotropy but also an additional two-fold anisotropy. This two-fold anisotropy increases on warming and probably expressed as $\cos 2(\phi_H - \phi_I)$, suggesting that flux flow resistivity generated by the Lorentz effect leads to underestimation of H_{c2} in the ab plane. We find another two-fold term behaving as $\sin 2\phi_H$, independent of the current direction. This component, indicative of the sensitivity of the superconductivity to sample inhomogeneity, becomes noticeable only below 0.8 K, where field-induced phases such as the FFLO state are highly anticipated.

Our study is expected to provide hints toward clarification of the remaining issues on Sr_2RuO_4 , such as the origin of the enhancement of T_c under uniaxial strain or in eutectic crystals, and the relationship between the superconducting order parameters and the anisotropy of H_{c2} . In addition, our resistivity measurement system will be helpful for investigating interesting phenomena in other materials such as coupling between current and electronic nematicity in nematic superconductors [31] or in nematic electron liquid systems [32].

ACKNOWLEDGEMENT

The authors thank Y. Yanase, K. Machida, K. Ishida, S. Kitagawa, G. Mattoni, for valuable discussions. We also acknowledge technical supports from Kyoto Univ. LTM Center. This work is supported by Japan Society for the Promotion of Science (JSPS) Core-to-core program (No. JPJSCCA20170002) and by JSPS KAKENHI Nos. JP15H05852, JP15K21717, JP17H06136, and JP20H05158. This work is also supported by Research Grants Council of Hong Kong (CUHK 14301316) and CUHK Direct Grants (No. 4053299, 4053345).

- [1] Y. Maeno, H. Hashimoto, K. Yoshida, S. Nishizaki, T. Fujita, J. G. Bednorz, and F. Lichtenberg, “Superconductivity in a layered perovskite without copper” *Nature* **372**, 532 (1994).
- [2] C. Bergemann, A. P. Mackenzie, S. R. Julian, D. Forsythe, and E. Ohmichi, “Quasi-two-dimensional Fermi liquid properties of the unconventional superconductor Sr_2RuO_4 ” *Adv. Phys.* **52**, 639 (2003).
- [3] A. Damascelli, D. H. Lu, K. M. Shen, N. P. Armitage, F. Ronning, D. L. Feng, C. Kim, Z.-X. Shen, T. Kimura, Y. Tokura, Z. Q. Mao, and Y. Maeno, “Fermi Surface, Surface States, and Surface Reconstruction in Sr_2RuO_4 ” *Phys. Rev. Lett.* **85**, 5194 (2000).
- [4] A. Pustogow, Y. Luo, A. Chronister, Y.-S. Su, D. A. Sokolov, F. Jerzembeck, A. P. Mackenzie, C. W. Hicks, N. Kikugawa, S. Raghu, E. D. Bauer, and S. E. Brown, “Constraints on the superconducting order parameter in Sr_2RuO_4 from oxygen-17 nuclear magnetic resonance” *Nature* **574**, 72 (2019).
- [5] K. Ishida, M. Manago, K. Kinjo, and Y. Maeno, “Reduction of the ^{17}O Knight Shift in the Superconducting State and the Heat-up Effect by NMR Pulses on Sr_2RuO_4 ” *Journal of the Physical Society of Japan* **89**, 034712 (2020).
- [6] A. Chronister, A. Pustogow, N. Kikugawa, D. A. Sokolov, F. Jerzembeck, C. W. Hicks, A. P. Mackenzie, E. D. Bauer, and S. E. Brown, “Evidence for even parity unconventional superconductivity in Sr_2RuO_4 ” *Proceedings of the National Academy of Sciences of the United States of America* **118**, 25 (2021).
- [7] A. N. Petsch, M. Zhu, M. Enderle, Z. Q. Mao, Y. Maeno, I. I. Mazin, and S. M. Hayden, “Reduction of the Spin Susceptibility in the Superconducting State of Sr_2RuO_4 Observed by Polarized Neutron Scattering” *Phys. Rev. Lett.* **125**, 217004 (2020).
- [8] G. M. Luke, Y. Fudamoto, K. M. Kojima, M. I. Larkin, J. Merrin, B. Nachumi, Y. J. Uemura, Y. Maeno, Z. Q. Mao, Y. Mori, H. Nakamura, and M. Sigrist, “Time-reversal symmetry-breaking superconductivity in Sr_2RuO_4 ” *Nature* **394**, 558 (1998).
- [9] J. Xia, Y. Maeno, P. T. Beyersdorf, M. M. Fejer, and A. Kapitulnik, “High Resolution Polar Kerr Effect Measurements of Sr_2RuO_4 : Evidence for Broken Time-Reversal Symmetry in the Superconducting State” *Phys. Rev. Lett.* **97**, 167002 (2006).
- [10] V. Grinenko, S. Ghosh, R. Sarkar, J.-C. Orain, A. Nikitin, M. Elender, D. Das, Z. Guguchia, F. Brückner, M. E. Barber, J. Park, N. Kikugawa, D. A. Sokolov, J. S. Bobowski, T. Miyoshi, Y. Maeno, A. P. Mackenzie, H. Luetkens, C. W. Hicks, and H.-H. Klauss, “Split superconducting and time-reversal symmetry-breaking transitions in Sr_2RuO_4 under stress” *Nature Phys.* **17**, 748 (2021).
- [11] V. Grinenko, D. Das, R. Gupta, B. Zinkl, N. Kikugawa, Y. Maeno, C. W. Hicks, H.-H. Klauss, M. Sigrist, and R. Khasanov, “Unsplit superconducting and time reversal symmetry breaking transitions in Sr_2RuO_4 under hydrostatic pressure and disorder” *Nature Communications* **12**, 3920 (2021).
- [12] S. Benhabib, C. Lupien, I. Paul, L. Berges, M. Dion, M. Nardone, A. Zitouni, Z. Q. Mao, Y. Maeno, A. Georges, L. Taillefer, and C. Proust, “Ultrasound evidence for a two-component superconducting order parameter in Sr_2RuO_4 ” *Nature Phys.* **17**, 194 (2021).
- [13] S. Ghosh, A. Shekhter, F. Jerzembeck, N. Kikugawa, D. A. Sokolov, M. Brando, A. P. Mackenzie, C. W. Hicks, and B. J. Ramshaw, “Thermodynamic evidence for a two-component superconducting order parameter in Sr_2RuO_4 ” *Nature Phys.* **17**, 199 (2021).
- [14] M. Ichioka, H. Adachi, T. Mizushima, and K. Machida, “Vortex state in a Fulde-Ferrell-Larkin-Ovchinnikov superconduc-

* araki.ryo.43w@st.kyoto-u.ac.jp

† yonezawa.shingo.3m@kyoto-u.ac.jp

tor based on quasiclassical theory" Phys. Rev. B **76**, 014503 (2007).

[15] P. Fulde and R. A. Ferrell, "Superconductivity in a Strong Spin-Exchange Field" Phys. Rev. **135**, A550 (1964).

[16] A. I. Larkin and Y. N. Ovchinnikov, Zh. Eksp. Teor. Fiz. **47**, 1136 (1964), [translation: Sov. Phys. JETP **20** (1965) 762].

[17] S. Yonezawa, T. Kajikawa, and Y. Maeno, "First-Order Superconducting Transition of Sr_2RuO_4 " Phys. Rev. Lett. **110**, 077003 (2013).

[18] S. Yonezawa, T. Kajikawa, and Y. Maeno, "Specific-Heat Evidence of the First-Order Superconducting Transition in Sr_2RuO_4 " J. Phys. Soc. Jpn. **83**, 083706 (2014).

[19] Z. Q. Mao, Y. Maeno, S. Nishizaki, T. Akima, and T. Ishiguro, "In-Plane Anisotropy of Upper Critical Field in Sr_2RuO_4 " Phys. Rev. Lett. **84**, 991 (2000).

[20] S. Kittaka, T. Nakamura, Y. Aono, S. Yonezawa, K. Ishida, and Y. Maeno, "Angular dependence of the upper critical field of Sr_2RuO_4 " Phys. Rev. B **80**, 174514 (2009).

[21] T. Matsushita, *Flux pinning in superconductors* (Springer, 2014).

[22] A. P. Mackenzie, R. K. W. Haselwimmer, A. W. Tyler, G. G. Lonzarich, Y. Mori, S. Nishizaki, and Y. Maeno, "Extremely Strong Dependence of Superconductivity on Disorder in Sr_2RuO_4 " Phys. Rev. Lett. **80**, 161 (1998).

[23] Z. Mao, Y. Maeno, and H. Fukazawa, "Crystal growth of Sr_2RuO_4 " Mater. Res. Bull. **35**, 1813 (2000).

[24] See Supplemental Material at [URL will be inserted by publisher] for [give brief description of material].

[25] S. Yonezawa, T. Higuchi, Y. Sugimoto, C. Sow, and Y. Maeno, "Compact AC susceptometer for fast sample characterization down to 0.1 K" Rev. Sci. Instrum. **86**, 093903 (2015).

[26] R. Loetzsches, A. Lübecke, I. Uschmann, E. Förster, V. Große, M. Thuerk, T. Koettig, F. Schmidl, and P. Seidel, "The cubic to tetragonal phase transition in SrTiO_3 single crystals near its surface under internal and external strains" Appl. Phys. Lett. **96**, 071901 (2010).

[27] O. Chmaissem, J. D. Jorgensen, H. Shaked, S. Ikeda, and Y. Maeno, "Thermal expansion and compressibility of Sr_2RuO_4 " Phys. Rev. B **57**, 5067 (1998).

[28] Y. Yasui, K. Lahabi, M. S. Anwar, Y. Nakamura, S. Yonezawa, T. Terashima, J. Aarts, and Y. Maeno, "Little-Parks oscillations with half-quantum fluxoid features in Sr_2RuO_4 microrings" Phys. Rev. B **96**, 180507 (2017).

[29] K. Deguchi, T. Ishiguro, and Y. Maeno, "Field-orientation dependent heat capacity measurements at low temperatures with a vector magnet system" Rev. Sci. Instrum. **75**, 1188 (2004).

[30] K. Kinjo, M. Manago, S. Kitagawa, Z. Q. Mao, S. Yonezawa, Y. Maeno, and K. Ishida, "Superconducting Spin Smecticity Evidencing the Fulde-Ferrell-Larkin-Ovchinnikov State in Sr_2RuO_4 " submitted (2021).

[31] S. Yonezawa, "Nematic Superconductivity in Doped Bi_2Se_3 Topological Superconductors" Condensed Matter **4** (2019), ISSN 2410-3896, doi:10.3390/condmat4010002.

[32] R. M. Fernandes, A. V. Chubukov, and J. Schmalian, "What drives nematic order in iron-based superconductors?" Nature Physics **10**, 97 (2014), ISSN 1745-2481.

**Supplemental Material for
Current-induced superconducting anisotropy of Sr_2RuO_4**

R. Araki,^{1,*} T. Miyoshi,¹ H. Suwa,¹ E. I. Paredes Aulestia,² K. Y. Yip,² K. T. Lai,² S. K. Goh,² Y. Maeno,¹ and S. Yonezawa^{1,†}

¹*Department of Physics, Kyoto University, Kyoto 606-8502, Japan*

²*Department of Physics, The Chinese University of Hong Kong, Shatin N.T., Hong Kong*

*araki.ryo.43w@st.kyoto-u.ac.jp

†yonezawa.shingo.3m@kyoto-u.ac.jp

(Dated: November 12, 2021)

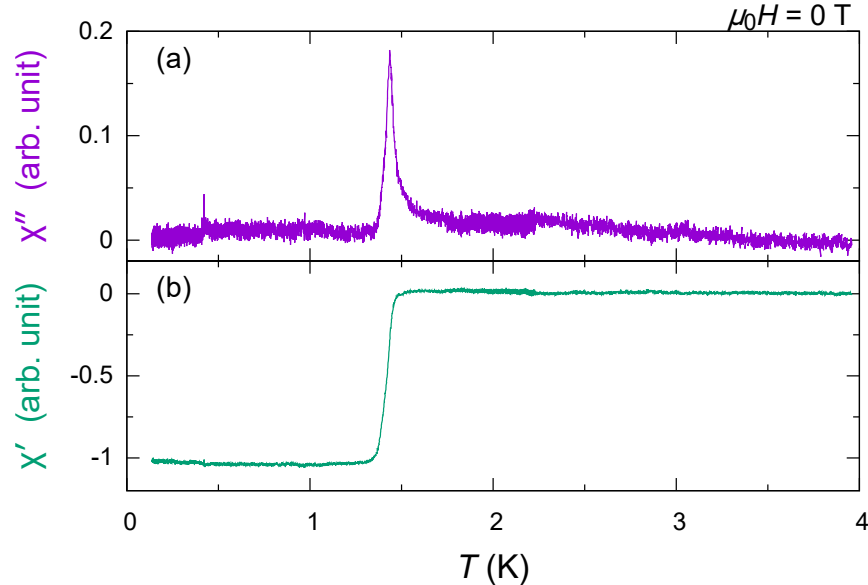


FIG. S1. AC susceptibility $\chi_{\text{ac}} \equiv \chi' - i\chi''$ of the Sr_2RuO_4 single crystal used for our device. Before the micro-fabrication, ac susceptibility measurement at zero DC field revealed that this thin crystal (batch: C432; $500 \mu\text{m} \times 100 \mu\text{m} \times 10 \mu\text{m}$) exhibits superconducting transition at $T_c = 1.43$ K, which is defined as the peak of the imaginary part of χ_{ac} .

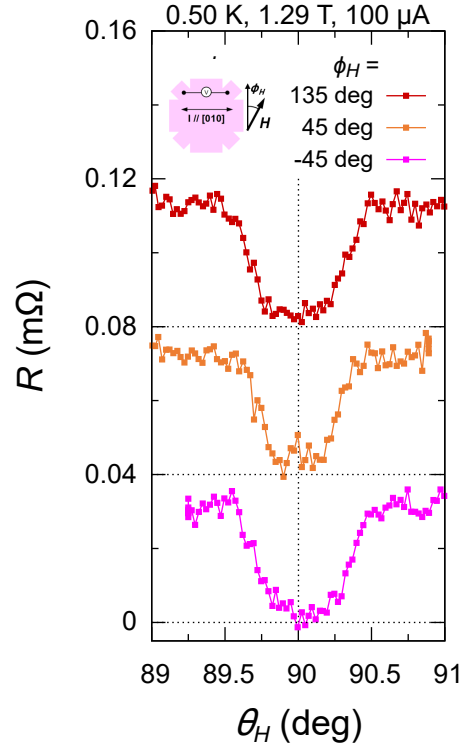


FIG. S2. Check of the alignment of magnetic field to the ab plane. The figure shows the polar-angle θ_H dependence of the resistance R measured at 0.50 K under 1.29 T and 100- μA current along the [010] direction. The curves have vertical offsets. The red, orange and pink curves correspond to $\phi_H = 135^\circ, 45^\circ$ and -45° , respectively. For all ϕ_H , $R(\theta_H)$ curves show sharp and symmetric dips centered at $\theta_H = 90^\circ$ due to superconductivity. These data indicate that the misalignment of the magnetic field with respect to the ab plane ($\theta_H = 90^\circ$) is at most 0.1° .

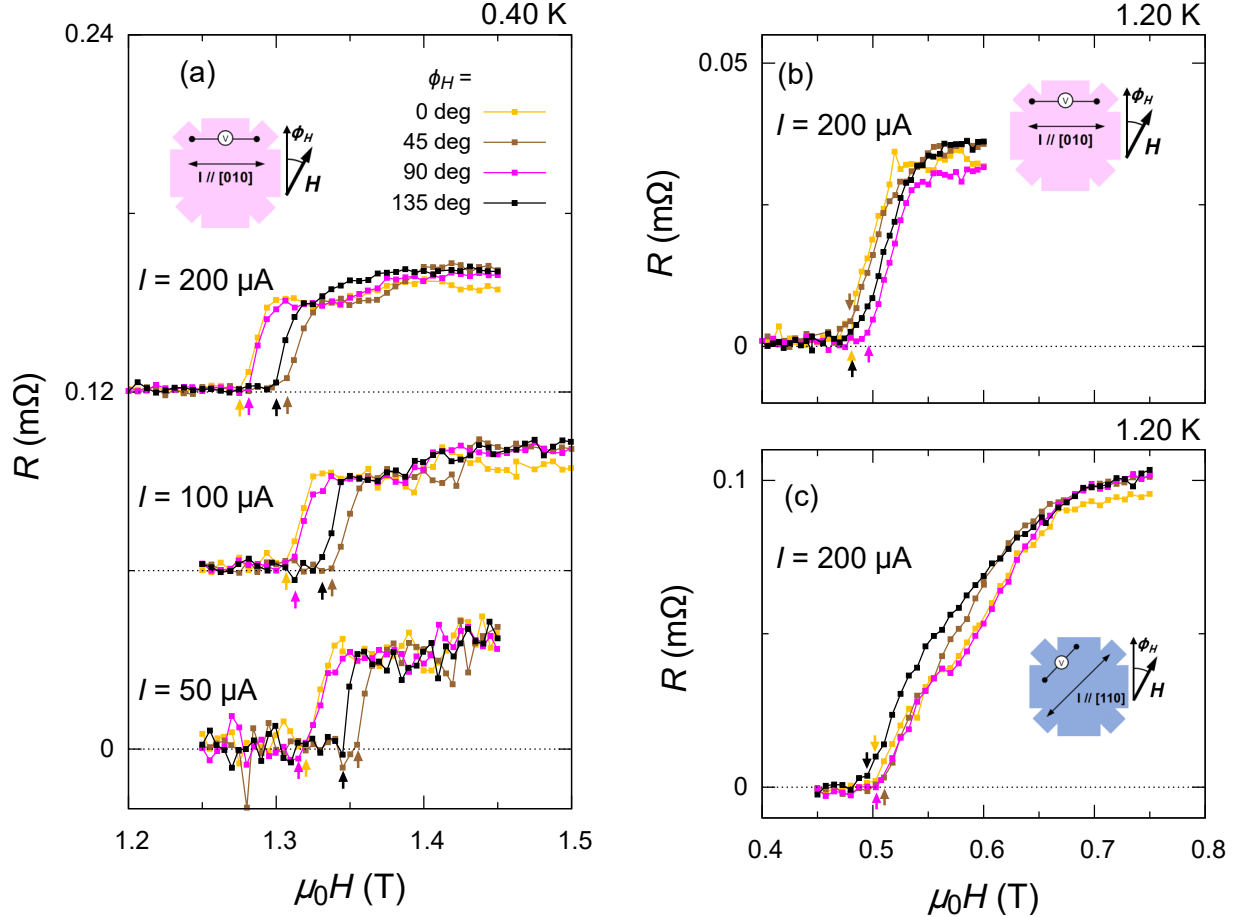


FIG. S3. Raw magneto-resistance data. The figure represents resistive transition of our Sr_2RuO_4 device under currents. The yellow, brown and black data points are obtained under $\phi_H = 0^\circ, 45^\circ, 90^\circ$ and 135° , respectively. (a) Data under currents along the $[010]$ direction at 0.4 K. Similarly to the $R(H)$ curves in Fig. 2 of the main text, H_{c2} , indicated by the vertical arrows, exhibits two-fold anisotropy as evidenced by the differences between the curves of $\phi_H = 0^\circ$ and 90° , or those of $\phi_H = 45^\circ$ and 135° . (b) Data under currents along the $[010]$ direction at 1.20 K, where superconducting transition is an ordinary second-order transition. (c) Data under currents along the $[110]$ direction at 1.20 K.

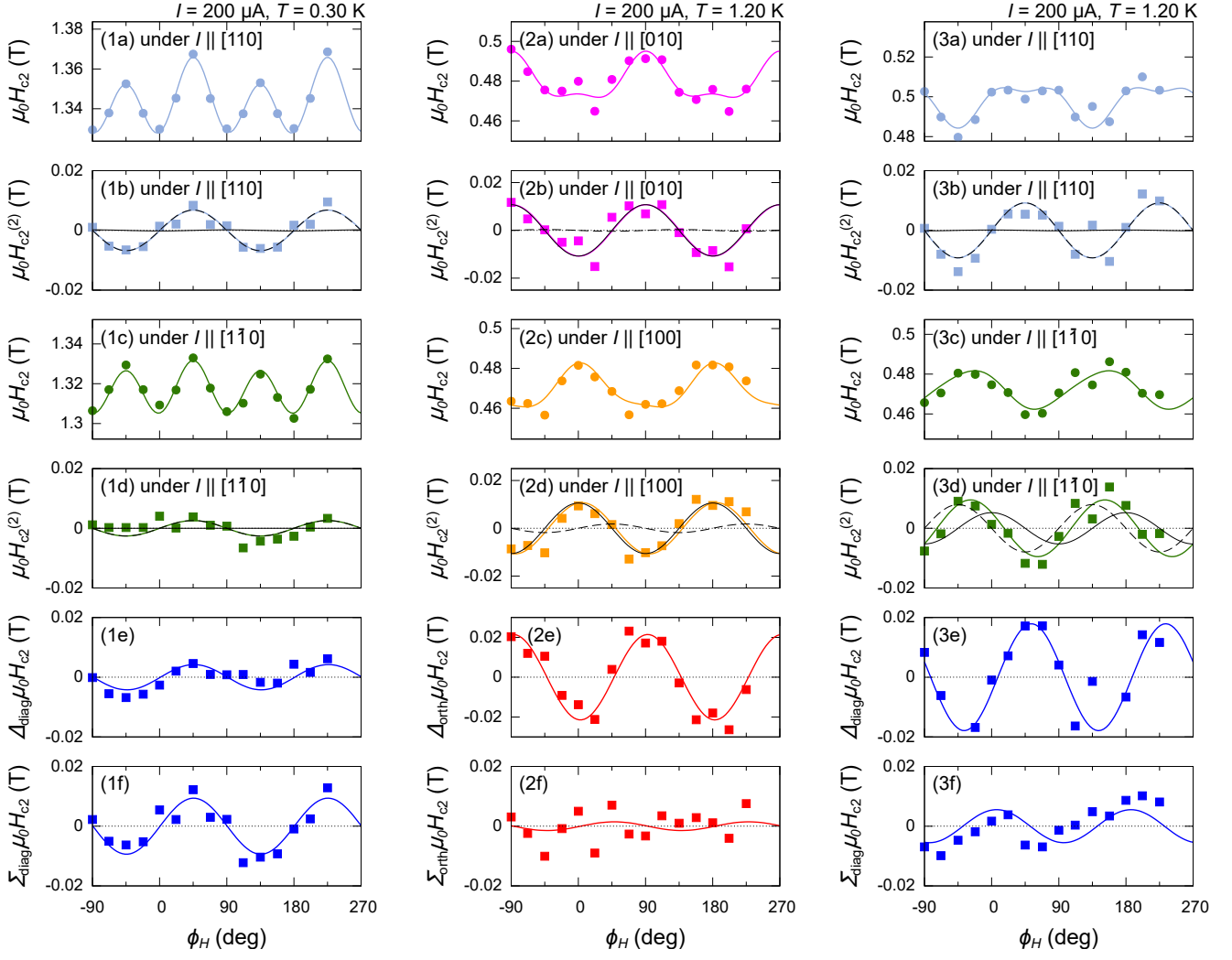


FIG. S4. Representative H_{c2} anisotropy of Sr_2RuO_4 under in-plane current. Similarly to Fig. 3 of the main text, (a) and (c) represent raw H_{c2} data (circles) and fitting result (solid curve) under current, (b) and (d) represent two-fold components of H_{c2} under current, extracted from the raw H_{c2} data by subtracting the fitted four-fold component and the constant offset, (e) represents I -induced two-fold component of H_{c2} obtained by taking the difference between the data in (b) and (d), and (f) represents I -independent two-fold component of H_{c2} obtained by taking the summation of the data in (b) and (d), respectively. The sky blue, green, pink and yellow color indicate data under current parallel to the [110], [110], [010] and [100] directions, respectively. The blue and red color indicate data evaluated from the datasets for the orthogonal and diagonal current-directions, respectively. Column (1) H_{c2} under currents along the diagonal directions at 0.30 K. Column (2) H_{c2} under currents along the orthogonal directions at 1.20 K. Column (3) H_{c2} under currents along the diagonal directions at 1.20 K.

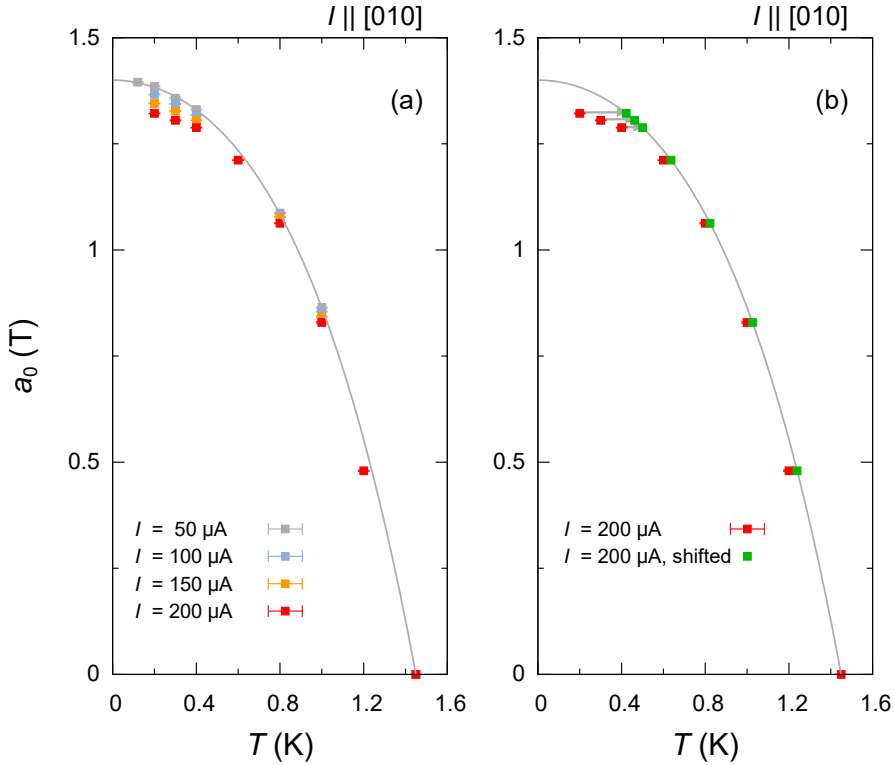


FIG. S5. Examination of heating effect from the T -dependence of the coefficient a_0 considered as the in-plane average H_{c2} . (a) Gray, sky-blue, yellow and red squares show a_0 measured with current strength $I = 50, 100, 150$ and $200 \mu\text{A}$ respectively. Gray curves shows the fitting curve obtained from the in-plane average H_{c2} measured with $50 \mu\text{A}$ (b) Red squares and gray curves show the same data as those in the panel (a). Green squares show the points with a_0 measured with $I = 200 \mu\text{A}$ shifted onto the fitting curve. To estimate the deference between the actual sample temperature and the measured temperature, we assume that the change in a_0 is caused only by Joule heating and the gray curves exhibits the ideal H_{c2} - T phase diagram of the sample. This estimation indicates the temperature increase as evaluated by the shift indicated by the gray arrows is at most 0.2 K in the lowest temperature region and less than 0.1 K above 0.4 K. Therefore, the current-heating effect has no qualitative effects on the analyses and conclusions.

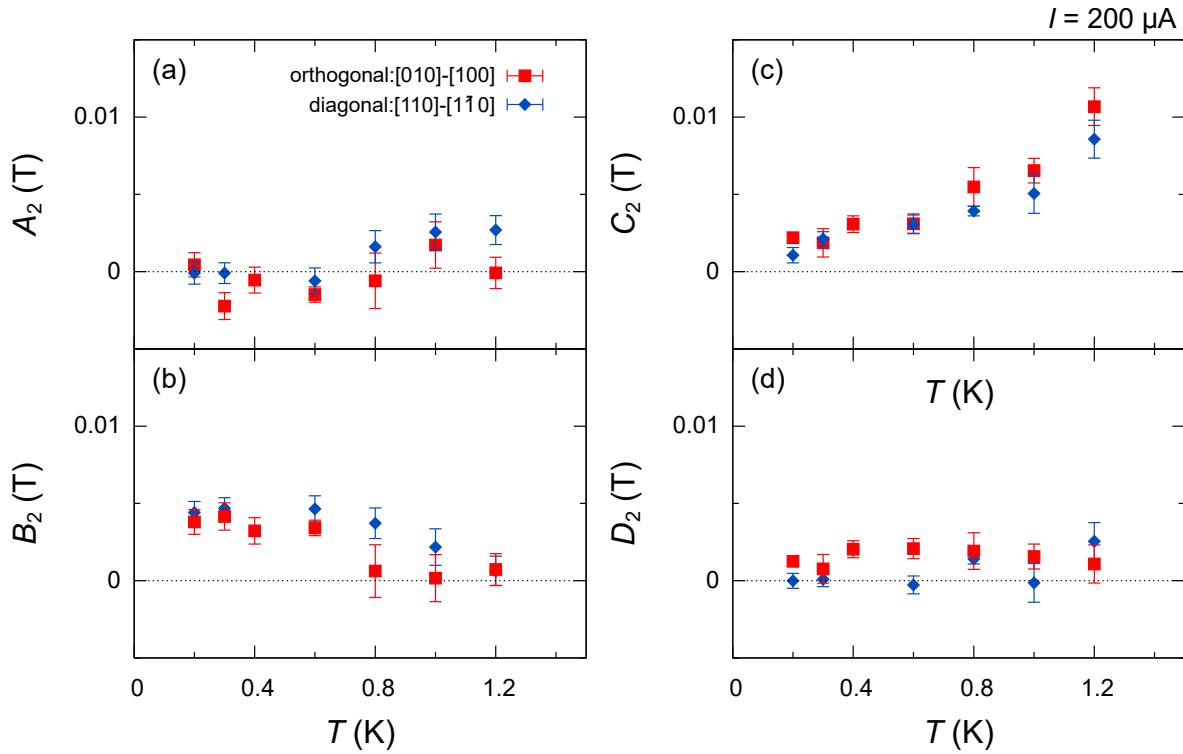


FIG. S6. T -dependence of the two-fold I -dependent component and I -independent component of $H_{c2}^{(2)}$. Red squares and blue diamonds indicate values evaluated from the datasets for the orthogonal and diagonal current-directions, respectively. B_2 and C_2 shown in the panels (b) and (c) respectively are the same as B_2 and C_2 in Fig. 5 of the main text. (a) Two-fold I -independent cosine component. This coefficient exhibits nearly zero at all temperatures. (b) Two-fold I -independent sine component. This coefficient shows about 0.005 T in the first-order transition region ($T \leq 0.8$ K) and nearly zero in the second-order transition region ($T \geq 0.8$ K). This fact implies that the sample in a high-field state gets sensitive to inhomogeneity effect producing two-fold anisotropy. (c) Coefficient for the $\cos 2(\phi_H - \phi_I)$ component, which increases on warming. It is consistent with vortex flow effect. (d) Coefficient for the $\sin 2(\phi_H - \phi_I)$ component, exhibiting nearly zero in the whole temperature range.